Detection of Internal and Overall Dynamics of a Two-Atom-Tethered Spin-Labeled DNA†

Robert S. Keyes and Albert M. Bobst*

Department of Chemistry, University of Cincinnati, Cincinnati, Ohio 45221

Received March 13, 1995⊗

ABSTRACT: DNA motions consist of several components which couple, making their investigation difficult. This study describes an approach for obtaining dynamical information by EPR when spin-labeled nucleic acids are examined. The analysis is accomplished by implementing two motional models. The first model (i.e., dynamic cylinder model) views the spin-labeled helix as a diffusing cylinder containing internal dynamics which are characterized by an order parameter. The second model (i.e., base disk model) provides correlation times describing the diffusion of the spin-labeled base. In each model, the nitroxide motion consists of both global and internal contributions. Dynamic cylinder and base disk simulations of four duplexes containing nitroxides attached to thymidine by a two-atom tether (DUMTA)—$(dT)_7$DUMTA-$(dT)_7$•$(dA)_{15}$, $[(dT)_7$DUMTA$(dT)_7]_2$•$(dA)_{30}$, $[(dT)_7$DUMTA$(dT)_7]_3$•$(dA)_{45}$, and $[(dT)_7$DUMTA$(dT)_7]_m$•$(dA)_n$—demonstrate the useful application of this approach. From dynamic cylinder simulations, the order parameter for internal motions is found to be independent of the helix length ($S = 0.32 \pm 0.01$). Previous base disk simulations of a DNA 26mer and polymer labeled with a five-atom-tethered nitroxide seemed to indicate that $\tau_\perp$ was only sensitive to internal dynamics. Results from base disk simulations of DUMTA-labeled DNA indicate that the perpendicular component of the base disk correlation time ($\tau_\perp = 1.4-6.2$ ns) is sensitive to global dynamics. Thus, $\tau_\perp$ is a quantitative indicator of both internal and global dynamics. Comparison of the two models reveals that $\tau_\perp \propto S^2\tau_{rb}$, where τ_{rb} represents the rigid-body diffusion of the DNA helix. This relationship between S and $\tau_\perp$ provides a framework for studying conformational changes and size-dependent phenomena in spin-labeled nucleic acids. Application of the dynamic cylinder model to a B−Z transition generates distinct values of S for each of the conformations, indicating that Z-DNA is more rigid than B-DNA.

It has been known for a long time that DNA does not simply exist in the static B-structure, but that it exists in other conformations as well (Wells, 1988). In addition, even within a given conformation, the equilibrium structure undergoes thermal fluctuations which drive various dynamical modes. Considerable effort has been expended in studying both the nature and rate of these motions. This work has resulted in a better understanding of the relationships between the structure, dynamics, and function of DNA.

The dynamics of DNA can be broken down into very specific contributions or modes (Tidor et al., 1983). For instance, the motion of an individual base consists of twisting, tilting, and torsional components. However, due to the difficulties inherent in separating these numerous contributions, motions are generally classified into sets of increasing scope. These include base oscillations (comprised of both small amplitude librations and large amplitude opening/closing reactions), multiple base opening breathing reactions, collective uniform bending and twisting modes, and global tumbling. All but the last of these sets of motions can be further grouped into the class of internal motions.

Wahl et al. (1970) were the first to detect internal oscillations within DNA. These motions were recognized by using fluorescence intercalators bound to the helix. Barkley and Zimm (1979) as well as Allison and Schurr (1979) developed coupled oscillator models and interpreted this motion primarily in terms of twisting of the DNA helix supplemented by a small amount of bending. These helix length-dependent dynamics are considered to consist of collective motion of the base pairs. However, the base pairs undergo independent fluctuations as well. These range from the small amplitude librations of the individual bases seen by EPR and NMR to large amplitude opening and closing reactions observed by hydrogen-exchange experiments (Englander & Kallenbach, 1984; Hartmann et al., 1986; Folta-Stogniew & Russu, 1994). In these modes, the base pair acts as two separate base oscillators where each strand behaves as a separate series of oscillators, with the sugar−phosphate backbone acting as the axis.

Patkowski et al. (1990) have summarized the results of several studies on the internal motions of nucleic acids. The reported values of the internal correlation time fall within the range of 0.02−4 ns. A difficulty arises in determining which dynamical modes are primarily being monitored in a particular experiment as well as the magnitude of their respective correlation times. The problem lies both in finding techniques that effectively monitor one or more of the motional modes and in determining theoretical models that adequately explain the resulting data. Experimental techniques that only detect very fast motions (e.g., <10 ps) or very slow motions (e.g., >10 ns) may be useful for monitoring individual motional modes. For example, de-

† Supported in part by NIH Grants GM 27002 (A.M.B.), S10-RR04191 (Shared Instrument Grant), and P41-RR01008-19 (National Biomedical ESR Center).

* Author to whom correspondence should be addressed.

⊗ Abstract published in *Advance ACS Abstracts,* July 1, 1995.

0006-2960/95/0434-9265$09.00/0

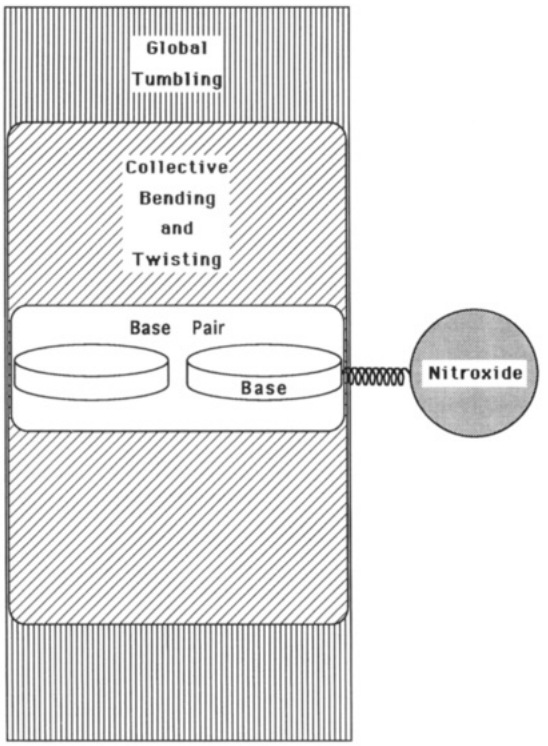

$$C_{NO/GT} = f(C_{NO/B}, C_{B/BP}, C_{BP/B\&T}, C_{B\&T/GT})$$

FIGURE 1: Coupling of the reporter group to various dynamical processes.

polarized dynamic light scattering (DDLS) can be used to measure the overall tumbling of a DNA helix apart from internal dynamics (Eimer et al., 1990). However, base librations, bending and twisting motions, and global tumbling (at least for oligomers) all have similar time scales such that the motions are coupled, resulting in a complex set of correlation functions (Figure 1). On the time scale of EPR, all of the main motional modes influence the spectral line shape. Currently, the options for dynamic analysis are either to attempt to fit experimental data to currently available functions or to perform some type of phenomenological analysis where it is not necessary to deconvolute the dynamics.

NMR has been an effective tool for monitoring these motions as well. A number of researchers have concluded that the dynamics of intrabase proton−proton vectors occur in the subnanosecond time scale with amplitudes of approximately 10−20° (Goljer & Bolton, 1994). However, the amplitude values strongly depend upon the geometry of the motional model employed. Therefore, the model-free approach of Lipari and Szabo (1982) has been used extensively to analyze NMR data and, in particular, to establish order parameters. These results are more general and can be further interpreted in terms of a specific model if desired. The square of the generalized order parameter S^2 has been determined to be about 0.8 for paired base carbons (Borer et al., 1994).

Using a spin-labeled acridine intercalator, Robinson et al. (1980) monitored the torsional motions with respect to amplitude and correlation time utilizing EPR. However, intercalators can cause large perturbations, and it is not always clear how well they are coupled to molecular motion. Ideally, the reporter group should effectively mimic the motion it is detecting while not disturbing that motion. Nitroxide spin labels attached to individual bases provide information about base dynamics without significantly influencing the system.

There are two approaches that have been used to quantify the motions of spin-labeled bases within DNA. Hustedt et al. (1993a) used an anisotropic model to analyze their EPR spectra, where the DNA helix was considered to be the diffusing system. Correlation times for the diffusion of a rigid cylinder were calculated by hydrodynamic theory. EPR data of oligomers of various lengths labeled with an acetylene-tethered nitroxide showed significant size dependence, which was interpreted in terms of bending and global tumbling. The internal dynamics consisting of collective bending motions, as well as individual base and spin-label motion, were taken into account by allowing the **g** and **A** tensors to average. They concluded that local spin-label motion consisted of uniaxial rotation about the acetylene-tether bond and that there is very little base motion in contrast to results obtained by other studies (Kao et al., 1983; Kao & Bobst, 1985; Pauly et al., 1987; Strobel et al., 1990a,b; Eimer et al., 1990). However, recent evidence indicates that the attachment of a propyne group to the C5 position of thymidine has the effect of stabilizing duplex DNA (Froehler et al., 1992). Considering that the melting curve of a 12mer spin-labeled with an acetylene-tethered nitroxide seems to indicate some amount of helix stabilization prior to dissociation (Spaltenstein et al., 1988), this stabilizing effect may provide a better solution to why an acetylene-tethered spin label does not detect base dynamics.

This laboratory has used an anisotropic model (Kao et al., 1983) characterized by two correlation times that describe diffusion around the principal axis, $\tau_{||}$,[1] and perpendicular to it, $\tau_{\perp}$ (Mason et al., 1974). The base is modeled as a disk (base disk model), which is distinguished from intercalator models that consider the base pair to be the disk. The assembly of the nitroxide tethered to the base is defined as the diffusing system. The principal diffusion axis is considered to coincide with an axis defined by the bond connecting the tether to the base. Actually, since the base itself diffuses, resulting in a change in position of the tether bond, the principal diffusion axis is an average of the tether bond positions. This model has been successfully applied to over 40 DNA and RNA systems with thymidylates and deoxycytidylates substituted in position 5 with nitroxides containing tethers varying in length from 2 to 11 atoms (Kao et al., 1983; Kao & Bobst, 1985; Pauly et al., 1987; Strobel et al., 1990b). A key element of this model is that base motion contributes significantly to the dynamics of the system. A $\tau_{\perp}$ of about 4 ns has been consistently observed in double-stranded polymers. From preliminary studies of a DNA 26mer and polymer spin-labeled with the five-atom-tethered nitroxide DUAT (Figure 2), it was concluded that this value was independent of the helix length (Bobst et al., 1988); however, more recent results reported in the present study using the two-atom-tethered label DUMTA (Figure 2)

[1] Abbreviations: B, line broadening; DUAT, 5-[3-(2,2,6,6-tetramethyl-1-oxypiperidine-4-carboxamido)prop-1-enyl]-2′-deoxyuridine; DUMTA, 5-{[((2,2,6,6-tetramethyl-4-piperidyl)-1-oxy)amino]methyl}-2′-deoxyuridine; EPR, electron paramagnetic resonance; τ_{rb}, dynamic cylinder rigid-body correlation time; $\tau_{||}$, base disk parallel correlation time; $\tau_{\perp}$, base disk perpendicular correlation time; $T_{||}$, parallel component of τ_{rb}; $T_{\perp}$, perpendicular component of τ_{rb}; θ_{bd}, base disk tilt angle; θ_{dc}, dynamic cylinder tilt angle; S, order parameter.

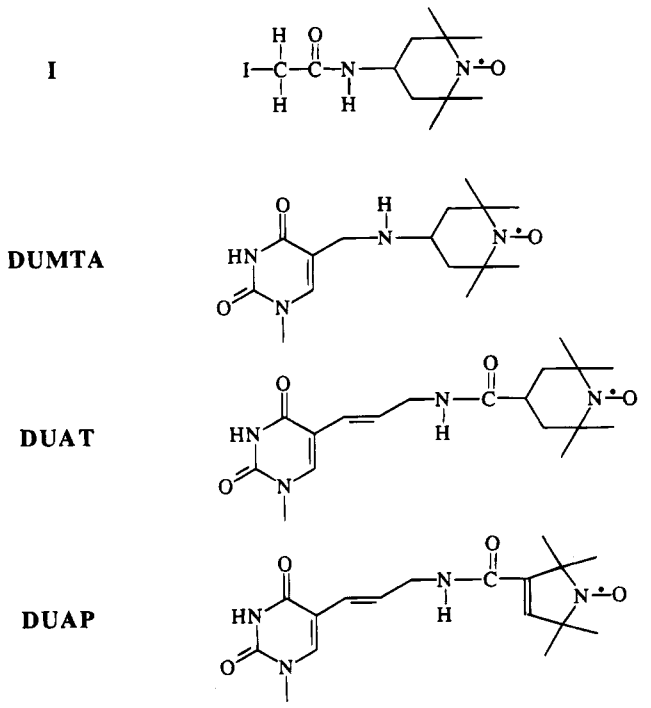

FIGURE 2: The chemical structures of the four spin labels discussed in the text.

indicate that $\tau_\perp$ does display some helix length dependence. This is because the overall motion of the base is caused by the helix length-dependent bending and twisting motions and global tumbling as well as the helix length-independent base dynamics which are all collectively represented by $\tau_\perp$. The faster of the correlation times $\tau_\parallel$ is tether dependent, is less than 1 ns, and is attributed to nitroxide motion that is independent of base motion. The value of $\tau_\parallel$ was found to decrease as the tether length increases, suggesting that long tethers are less rigid than short tethers.

In this work, the order parameter for internal motions determined by dynamic cylinder simulations is found to be independent of the helix length ($S = 0.32 \pm 0.01$). Results from base disk simulations indicate that $\tau_\perp$ (1.4−6.2 ns) is sensitive to both internal and global dynamics. The empirical relationship $\tau_\perp \propto S^2\tau_{rb}$ is found to exist between the two models (τ_{rb} is the rigid-body correlation time of the DNA helix). This proportionality establishes a foundation for studying conformational changes such as the B−Z transition and size-dependent phenomena including protein binding.

THEORY

Rigid-Limit Tensors. The primary difficulty encountered when measuring the rigid-limit magnetic tensors of spin labels is that the environment surrounding the nitroxide will almost certainly be different from that found in standard spin-labeling applications (i.e., dilute aqueous solution). The **g** and **A** tensor values are sensitive to features of the general environment including solvent polarity and hydrogen bonding (Hwang et al., 1975). An additional concern is that residual motion will lead to partial averaging of the rigid-limit values. The goal in determining rigid-limit tensor values is to restrict motion without significantly changing the environment.

One method that has been used successfully for extracting this information is to measure the EPR spectra of crystals along each of the principal magnetic axes, allowing the **g** and **A** tensor elements to be read directly from the spectra (Berliner, 1976). This avoids any residual motion and is effective for some nitroxides, but it is often impractical for spin-labeled systems and does not account for solvent effects. Another approach is to place the spin label in water and either freeze or lyophilize the sample in order to restrict motion while at the same time providing solvent interactions. A major concern with this technique is the formation of hydrogen bonds in the solid phase (Hustedt et al., 1993a). The method chosen in this paper is to place the spin label in a highly viscous aqueous solution, lower the temperature, and measure the spectra of the randomly oriented species near the rigid limit of the linear EPR time scale ($\tau > 10^{-6}$ s). Although care must be taken to ensure that residual motion will not affect the tensor values, the solvent environment is much closer to standard experimental conditions. Glycerol was chosen over sucrose as the solute due to its small molecular size relative to the spin labels.

Routine EPR measurements of spin-labeled systems are generally accomplished using X-band frequencies (9.8 GHz). Analyses of rigid-limit X-band spectra provide values for the principal tensor elements g_{zz} and A_{zz}. These values can be readily obtained since the upfield and downfield z-turning points do not overlap with the other resonance peaks. However, the x and y turning points do overlap, and the magnetic parameters must be extracted from the spectra by simulation. Higher frequency resonance increases the separation between the peaks due to the fact that the **g** tensor anisotropy increases (Griffith & Jost, 1976). Q-band measurements (35 GHz) provide enough resolution to allow values for g_{yy}, g_{zz}, A_{yy}, and A_{zz} to be read directly from the spectra. Although it was once a common practice to obtain g_{xx} and A_{xx} directly from the x-spectral turning points, detailed analysis indicates that they must be extracted by simulation (Pasenkiewicz-Gierula et al., 1983).

Spin-labeled thymidylate analogs incorporated into nucleic acids have been used for determining protein binding affinities (Keyes & Bobst, 1993), developing hybridization assays (Strobel et al., 1991), and monitoring conformational changes (Kao & Bobst, 1985; Strobel et al., 1990b; Spaltenstein et al., 1989). The values of the magnetic **g** and **A** tensors that have been used for past simulations of the various six-membered ring nitroxide spin labels prepared in this lab were originally determined for 4-(2-iodoacetamido)-2,2,6,6-tetramethylpiperidinyloxyl (**I**) (Figure 2 and Table 1) (Bobst, 1979; Pan, 1975). However, it has become necessary to remeasure these values due to the possible differences in gaussmeter and frequency meter calibration between the two EPR spectrometers (Varian E-104 and Bruker ESP 300) now used in this laboratory and in order to extend the analysis of spin-labeled systems. Determination of the dynamic cylinder and base disk parameters requires accurate and consistent values for the rigid-limit magnetic tensors. The EPRFIT spectral fitting program which generates simulations that closely conform to the experimental data has facilitated these determinations.

DNA Dynamics. The EPR spectrum of a rapidly diffusing nitroxide spin label can be described by a superposition of Lorentzian lines representing distinct resonance frequencies generated by hyperfine splitting of the paramagnetic electron energy level. The magnetic tensor anisotropy is completely averaged, resulting in a spectrum with three sharp lines. Dynamical information can be readily extracted by measuring

Table 1: Spin Label Magnetic Tensor Values[a]

compd	g_{xx}	g_{yy}	g_{zz}	$\bar{g}$	$^1/_3$Tr **g**	A_{xx} (G)	A_{yy} (G)	A_{zz} (G)	$\bar{A}$ (G)	$^1/_3$Tr **A** (G)
DUMTA	2.0096	2.0067	2.0028	2.0063	2.0064	7.47	7.21	36.3	16.9	17.0
DUAT	2.0096	2.0067	2.0028	2.0064	2.0064	7.47	7.49	36.9	17.0	17.3
DUAP	2.0090	2.0066	2.0029	2.0062	2.0062	6.25	5.70	36.0	16.1	16.0
I	2.0088	2.0059	2.0026		2.0058	7.15	7.35	35.6	16.7	16.7

[a] In general, errors in hyperfine splitting values are reported to be ±0.5 G while g value tolerances vary from ±0.0001 to ±0.0005 (Hustedt et al., 1993a; Pasenkiewicz-Gierula et al., 1983). However, this much variation would degrade the quality of the simulations.

the peak widths and heights (Nordio, 1976). However, if the motion is slow enough to be outside the motional narrowing region, then the spectrum becomes a complicated function of the dynamics which accumulate and contribute to the diffusion of the nitroxide, and extracting information about the dynamics is not straightforward. The spin label mobility is coupled to base oscillations which are coupled to torsions and flexures of neighboring bases which in turn are coupled to the global helical tumbling (Figure 1). This problem can be solved by using a simulation program that takes into account orientation dependence. In order to analyze the local mobility of the nitroxide without overinterpreting the data, the results will be quantified by separating the motions into two classes—internal dynamics and global tumbling. A complete analysis of this type for EPR spectra has been developed by the Freed group into a theoretical framework termed the slowly relaxing local structure (SRLS) model (Polnaszek & Freed, 1975; Freed, 1977; Zager & Freed, 1982). The internal dynamics are characterized by an order parameter and an internal correlation time describing a spin label rapidly diffusing within a local structure that relaxes on a longer time scale. The model-free approach of Lipari and Szabo (1982) developed for NMR addresses this problem as well; however, the global tumbling of the DNA helices in this work is slow motional and precludes a model-free analysis of our EPR data.

Ongoing effort is being made to apply the SRLS model to our systems. Currently, the internal dynamics will be described by developing a proportional relationship between the two axially symmetric motional models described in the introduction. The purpose behind this dual approach is to obtain an order parameter from the first model and the correlation times $\tau_{\|}$ and $\tau_{\perp}$ from the second (Steinhoff, 1988). The order parameter S, which is related to the usual order parameter definition $\langle P_2(\cos\theta)\rangle$ (where P_2 is the second Legendre polynomial) for axially symmetric dynamics (Griffith & Jost, 1976), is a measure of the degree of spatial restriction ranging from completely unrestricted ($S = 0$) to entirely restricted ($S = 1$). In this case, it indicates the amount of local ordering of the spin-labeled base. $\tau_{\|}$ and $\tau_{\perp}$ quantify the rate of spin-labeled base motion about and perpendicular to the diffusion axis. The total motion of the label within the helix will consist of internal motions augmented by overall tumbling. Therefore, the correlation times will be sensitive to both local and global effects. The analysis is accomplished by combining two simulation methods—one for each model—both using a simulation program based upon the Stochastic Liouville Equation. These two simulation approaches correspond to the two ways in which motional effects can be introduced into the simulation program.

Dynamic Cylinder Model. The first model pictures the DNA helix as a diffusing cylinder containing internal motions

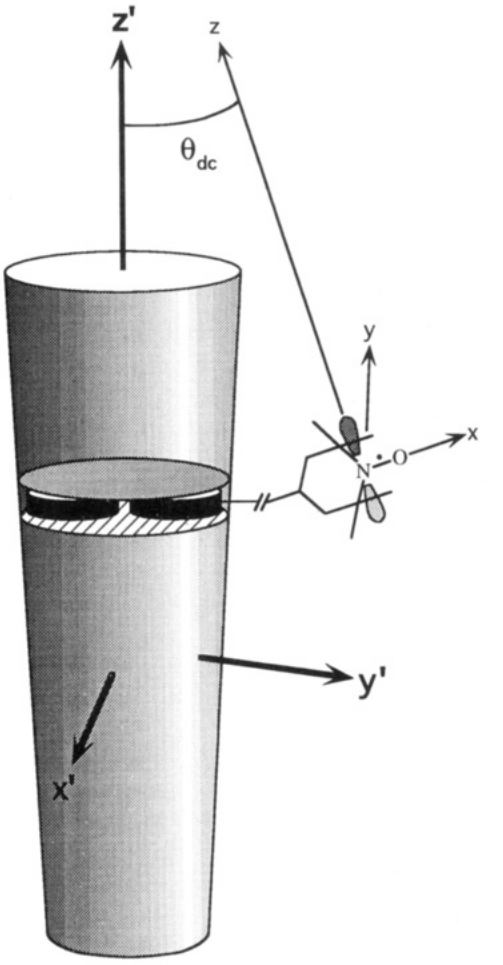

FIGURE 3: The magnetic (x, y, z) and diffusion (x', y', z') coordinates for the dynamic cylinder model. θ_{dc} represents the dynamic cylinder tilt angle.

(Figure 3) (Hustedt et al., 1993a). Accordingly, $\tau_{\|}$ and $\tau_{\perp}$ represent diffusion of the helical axis. The internal motions, which consist of both helix length-independent base dynamics and helix length-dependent bending and twisting, are characterized by averaging the principal values of the **g** and **A** tensors. This approach to motional separation is valid when the internal dynamics are fast. In other words, the correlation times must be faster than about 10^{-9} ns (Nordio, 1976). This upper limit is actually higher since the internal motions are limited in amplitude, thus increasing the correlation of the molecular orientations (Hustedt et al., 1993a).

The concept of magnetic tensor averaging has been utilized by many researchers to account for dynamics (Van et al., 1974; Griffith & Jost, 1976; Zimmel, 1983; Hustedt et al., 1993a). The greater the rate of motion, the greater the averaging. The hyperfine tensors for a static crystal or for molecular diffusion in the rigid-limit region are A_{xx}, A_{yy}, and A_{zz}. A species is axially symmetric either when the rigid-limit A_{xx} and A_{yy} tensors are nearly equal or when fast rotation

about the z axis averages A_{xx} and A_{yy} together into $A_\perp$ resulting in $A_{zz} = A_{||}$ and $A_{xx} = A_{yy} = A_\perp$. Partial averaging can refer to either spatial or temporal averaging. For instance, when Van et al. (1974) use the term partial averaging, they mean a spatially restricted averaging in the fast motional limit, whereas Steinhoff (1989) uses the term to mean averaged between the rigid and fast limits. When complete averaging occurs, then an isotropic value is reached where:

$$\bar{A} = {}^1/_3(A_{xx} + A_{yy} + A_{zz}) = {}^1/_3(A_{||} + 2A_\perp) \quad (1)$$

As averaging occurs, the tensor values are essentially pulled toward the isotropic value. This averaging concept applies to the **g** tensor as well; however, it is the **A** tensor that is generally used for quantitative purposes.

Since the **A** tensor can change as a result of both motional averaging and environment, care must be taken in determining the actual cause. A useful property that can aid in solving this problem is that second-order tensors are rotationally invariant (Steinhoff, 1988). This means that the trace of **A** will not change as a result of motional averaging. However, if hydrogen bond interactions or polarity changes occur, the trace will change and be correlated to the change in spectral splitting.

The purpose of this simulation method is to provide the order parameter S. The diffusion coefficients are determined by hydrodynamic theory, which models the diffusion rate in terms of a solvent with given viscosity and temperature acting upon an object of a particular geometry and size. In this case, the DNA helix is modeled as a cylinder; however, hydrodynamic equations have been developed for spheres, ellipsoids, dumbbells, and bent rods as well (García de la Torre & Bloomfield, 1981).

Schurr and Schmitz (1986) reported that diffusion data for tobacco mosaic virus follows the hydrodynamic theory of Tirado and de la Torre (1980) better than that of Broersma (1960). Tirado and de la Torre (1980) derived equations for the diffusion coefficients of a right circular cylinder:

$$D_\perp = \frac{[\ln(p) + \delta_1](3kT)}{\pi\eta L^3} \quad (2)$$

$$D_{||} = \frac{kT}{(1 + \delta_2)A\pi\eta LR^3} \quad (3)$$

where δ_1 and δ_2 are defined according to the parametrization of Spaltenstein et al. (1989):

$$\delta_1 = -0.661 + 0.891(p^{-1}) \quad (4)$$

$$\delta_2 = 0.688(p^{-1}) - 0.202(p^{-2}) \quad (5)$$

and:

$$p = (L/2R) \quad (6)$$

The remaining parameters are Boltzmann's constant (k), temperature (T), viscosity (η), cylinder length (L), and cylinder radius (R). The constant A equals 3.841. The correlation times for global tumbling are obtained from the diffusion coefficients, defined by eqs 2 and 3, according to:

$$T_i = \frac{1}{6D_i} \quad (7)$$

where i represents either $\perp$ or $||$. Steinhoff (1988) defines S in terms of the **A** tensor as:

$$S = \frac{\sum_{i=x,y,z} |A'_{ii} - {}^1/_3 TrA'|}{\sum_{i=x,y,z} |A_{ii} - {}^1/_3 TrA|} \quad (8)$$

where the A_{ii} are the crystal values and the A'_{ii} are the averaged values.

The order parameter can also be defined in terms of the z-component of the **A** tensor:

$$S_z = \frac{|A'_z - {}^1/_3 TrA'|}{|A_z - {}^1/_3 TrA|} \quad (9)$$

A rigid body correlation time will be defined that will be useful in comparing the results from the two motional models. Woessner (1962) developed a power spectrum expression for axially symmetric diffusion. Eimer et al. (1990) published the corresponding correlation function:

$$C_0(t) = \sum_{n=-2}^{2} A_n \exp\{-[6D_\perp + n^2 (D_{||} - D_\perp)]t\} \quad (10)$$

where the amplitude factors A_n are:

$$A_0 = {}^1/_4(3\cos^2\theta_{dc} - 1)^2 \quad (11a)$$

$$A_{\pm1} = {}^3/_2(\cos^2\theta_{dc})(1 - \cos^2\theta_{dc}) \quad (11b)$$

$$A_{\pm2} = {}^3/_8(\cos^2\theta_{dc} - 1)^2 \quad (11c)$$

and θ_{dc} is the dynamic cylinder tilt angle. Quantitatively, the correlation time is defined as the integral of the correlation function:

$$\tau = \int_0^\infty C(t)\, dt \quad (12)$$

Substituting eq 10 into eq 12 yields the corresponding rigid-body correlation time:

$$\tau_{rb} = A_0(6D_\perp)^{-1} + 2A_{\pm1}(D_{||} + 5D_\perp)^{-1} + 2A_{\pm2}(4D_{||} + 2D_\perp)^{-1} \quad (13)$$

Base Disk Model. The second model considers the spin-labeled base to be the axially symmetric diffusing system (Figure 4) (Kao et al., 1983) rather than the DNA helix. The rigid-limit values for the **g** and **A** tensors are used while varying the correlation times to account for motion. The principal diffusion axis coincides with the bond connecting the spin label to the base. $\tau_\perp$ represents all motions contributing to the motion of the labeled base including global tumbling.

Simulation Program. One very popular program TILT was developed by the Freed group (Polnaszek, 1976) and is based upon the Stochastic Liouville Equation (SLE) which describes the time evolution of an ensemble of resonating particles of various orientations. The SLE treats the electron transitions quantum mechanically while the orientation of the molecule is described by a classical stochastic process.

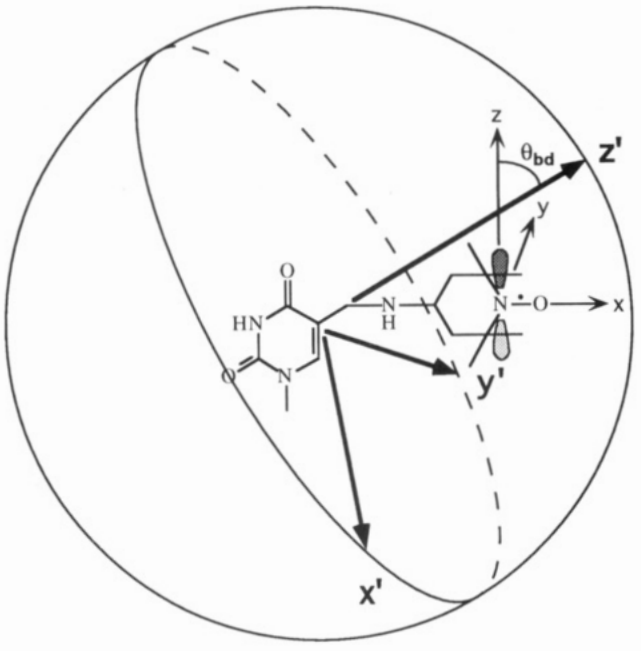

FIGURE 4: The magnetic (x, y, z) and diffusion (x', y', z') coordinates for the base disk model. θ_{bd} denotes the base disk tilt angle.

In this work, TILT is set to model the motion as axially symmetric Brownian diffusion.

TILT and related EPR spectral simulation programs (Polnaszek, 1976; Freed, 1976) have been popular for many years but previously required large mainframe computer facilities in order to completely diagonalize the program's matrices. With the advent of both powerful personal computers and improved computational algorithms, it has become possible to perform simulations quickly and efficiently (Schneider & Freed, 1989a,b). The programs simulate slow motion spectra by solving the SLE for select models of diffusion.

Experimental spectra are simulated in this paper utilizing the EPRFIT program (Hustedt et al., 1993b) which incorporates the TILT program as a subroutine. The input parameters for the program are the magnetic tensors **g** (i.e., g_{xx}, g_{yy}, g_{zz}) and **A** (i.e., A_{xx}, A_{yy}, A_{zz}), the correlation times $\tau_{\|}$ and $\tau_{\perp}$, the tilt angle θ, and the line broadening B. These last two parameters require additional explanation.

The tilt angle θ is one of the three Euler angles representing rotation of an object about a fixed point in a spherical coordinate system. In EPR, it is defined as the angle between the principal magnetic axis and the principal diffusion axis (Kao et al., 1983). Mathematically, it enters into the correlation function between the spin label and the diffusing molecule (Spaltenstein et al., 1989). Essentially, the tilt angle allows the coordinate systems of the spin label and molecule to be rotated with respect to one another. Since the EPR spectrometer only detects motion of the spin label, the correlation times determined by simulation must be corrected to reflect motion with respect to the molecular diffusion axis. The other two Euler angles ψ and ϕ generally have a small influence on the X-band EPR spectrum (Griffith et al., 1965).

The line broadening B accounts for additional terms in the Hamiltonian associated with nuclei other than the nitroxide nitrogen, primarily protons, coupling to the paramagnetic electron. Although these interactions are sometimes resolved into additional splittings, they generally have the effect of simply broadening the lines of the spectrum. Line broadening is assumed to arise from T_2 relaxation effects which are rotationally invariant. The relationship between B and T_2 is given by Polnaszek (1976) as:

$$B = \frac{(2/3^{0.5})T_2^{-1}}{|\gamma_e|} \tag{14}$$

where $\gamma_e = 1.7608425 \times 10^7$ rad/(s·G).

Broadening effects can become complicated, and experiments can be performed in an attempt to measure the various components of broadening (Bales, 1989). For instance, the EPRFIT program (Hustedt et al., 1993b) contains terms for Gaussian or Lorentzian broadening of the entire spectrum, T_{2e} broadening, Lorentzian broadening of individual lines, and anisotropic Lorentzian broadening of individual peaks within lines.

MATERIALS AND METHODS

Rigid-Limit Measurements. The individual spin labels were prepared as previously described (Kryak, 1990; Toppin et al., 1986; Pauly et al., 1989). For the isotropic measurements, approximately 5×10^{-5} M of either the DUMTA, DUAT, or DUAP mononucleotides was placed in a buffer consisting of 0.1 M NaCl and 0.01 M sodium cacodylate at pH 7.0. The rigid-limit samples were prepared with 2×10^{-4} M spin label in a 75% (w/w) glycerol aqueous solution.

Samples representing isotropic and rigid-limit dynamics were measured at X-band. The X-band EPR spectra were recorded on a Bruker ESP 300 spectrometer fitted with an ER 4111 VT variable temperature controller. The instrument parameters were as follows: modulation amplitude 0.8 G; modulation frequency 100 kHz; microwave power 5 mW; sweep width 100 G; conversion time 82 ms; time constant 82 ms. The receiver gain was between 5×10^4 and 2×10^5 for isotropic measurements and was within the range of $(1-2) \times 10^6$ for rigid-limit determinations.

The isotropic $\bar{g}$ and $\bar{A}$ values (Table 1) were determined from spectra taken at room temperature. Because the frequency meter only provides three significant figures, the $\bar{g}$ value was determined relative to a chromium standard (Cr^{3+} in a polyethylene matrix) (Bobst et al., 1984) according to the relationship:

$$g_{NO} = g_{Cr} \times \frac{H_{Cr}}{H_{NO}^{CF}} \tag{15}$$

where H_{Cr} is the field value of the major peak of Cr^{3+}, H_{NO}^{CF} is the field value of the nitroxide centerfield peak, and $g_{Cr} = 1.9804 \pm 0.0002$. The value for $\bar{A}$ was taken as the difference between the centerfield line and either the upfield or downfield line (a comparison was made to ensure that both splittings had the same magnitude).

The rigid-limit g_{zz} and A_{zz} tensor elements (Table 1) were measured from X-band spectra taken at 233 K (−40 °C). The difference between the upfield and downfield extrema corresponds to $2A_{zz}$, and the midpoint between the two extrema coincides with g_{zz} (Figure 5). The value for g_{zz} was established relative to a chromium standard according to eq 15.

Q-band measurements were performed on rigid-limit samples (−40 °C) at the National Biomedical ESR Center (Milwaukee, WI) on a Varian E-110 Q-band spectrometer.

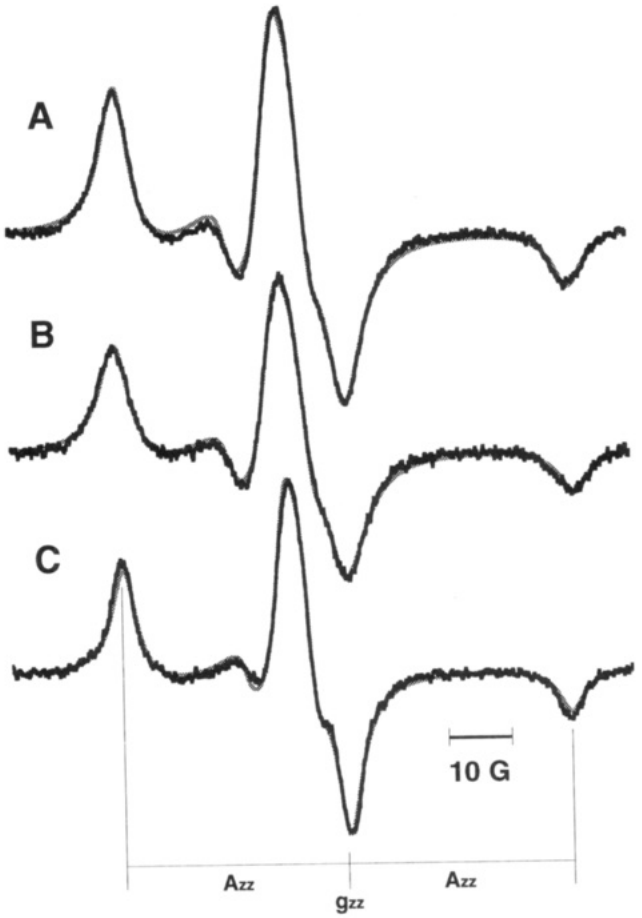

FIGURE 5: X-band EPR spectra (100 G scan) of (A) DUMTA, (B) DUAT, and (C) DUAP. Experimental spectra are indicated by a solid black line while simulations are denoted by a gray line.

The original microwave bridge has been modified (Hyde et al., 1991) to significantly increase EPR sensitivity. Instrument parameters were as follows: modulation amplitude 5 G; modulation frequency 100 kHz; microwave power 0.2 mW; sweep width 200 G; time constant 100 ms; receiver gain 3.2×10^2.

The EPR spectra were simulated using the EPRFIT program. The X-band data were fit by fixing g_{zz} and A_{zz} to the values obtained directly from the experimental spectra and varying the seven parameters g_{xx}, g_{yy}, A_{xx}, A_{yy}, and a Lorentzian broadening term for each of the three resonance lines. However, broadening was kept the same for all three lines of a given spin label. X-band linewidths were 2.8 G for DUMTA, 3.0 G for DUAT, and 2.4 G for DUAP. The Q-band spectra were simulated by fixing the principal g and A elements to the values determined by X-band and allowing only the Lorentzian linewidth to vary. Q-band linewidth broadening was 2.7 G for DUMTA, DUAT, and DUAP. The standard assumption was made that the **g** and **A** tensor axes coincide.

DNA Dynamics. The spin-labeled DNA molecules were synthesized according to published procedures from the Bobst laboratory. $(dT)_7DUMTA(dT)_7$ was constructed by the phosphotriester technique (Kryak & Bobst, 1990). The DUMTA-labeled 15mer was hybridized to $(dA)_{15}$, $(dA)_{30}$, $(dA)_{45}$, and $(dA)_n$ in a 0.1 M NaCl/0.01 M sodium cacodylate/0.01 M $MgCl_2$, pH 7.0 buffer to generate the corresponding duplexes. All EPR spectra were measured on a Bruker ESP 300 spectrometer.

EPR Simulations. All simulations were performed with the EPRFIT nonlinear fitting program utilizing either the TILT algorithm for axially symmetric diffusion or a rigid-limit subroutine (Hustedt et al., 1993b). The program is written in FORTRAN 77 compatible with the MS-DOS environment. Subsequent to obtaining the EPRFIT program, the source code was modified both to allow the **g** and **A** tensors to be fit and to establish compatibility with the Absoft FORTRAN 77 compiler. Because of the inherent memory limitations of MS-DOS, the Phar Lap 386|DOS Extender was used to link the programs into an executable file capable of accessing the additional memory required by the EPRFIT program. The calculations were performed on a 486DX2-based computer running at 66 MHz and containing 16 MB RAM.

Dynamic Cylinder Simulations. The dynamic cylinder simulations of the oligomers were performed with the TILT routine using the Tirado and de la Torre correlation times (eqs 2, 3, and 7). The **g** and **A** tensors, tilt angle, and broadening were allowed to vary. The polymer simulations were run with the rigid-limit subroutine since the correlation times for global tumbling were considered to be greater than 1000 ns.

Base Disk Simulations. All simulations for the base disk model were calculated using the TILT algorithm. The **g** and **A** tensors were fixed to the rigid-limit values determined by experiment. $\tau_{||}$, θ, and B were fixed to values in accordance with previous simulations. $\tau_{\perp}$ alone was allowed to vary.

RESULTS

Rigid-Limit Tensors. The results of rigid-limit measurements for three spin-labeled mononucleotides (Figure 2) are reported here. DUMTA (Kryak, 1990) and DUAT (Toppin et al., 1986) are both thymidylate analogs substituted in position C5 with six-membered ring nitroxides covalently attached by two- and five-atom tethers, respectively. DUAP (Pauly et al., 1989) is analogous to DUAT except that it contains a five-membered ring nitroxide. These three spin labels were chosen in order to monitor the effects of tether length and changing from a six- to five-membered ring nitroxide. In addition, these tensor values will be used in future analyses.

The spectral overlays of Figure 5 demonstrate the good conformity between the simulations and the X-band experimental data. The Q-band simulations (Figure 6) were generated using the **g** and **A** tensor values determined by X-band due to the fact that the two machines gave slightly different values for the **g** and **A** tensor elements. This resulted from the practical limitations of measuring field values in two different laboratories and had nothing to do with the fact that they operated at different frequencies. However, examination of Figure 6 clearly indicates that the simulations correspond well with the line-shape features of the Q-band spectra. The X-band values were given priority over the Q-band results since the experiments performed in this lab utilize the X-band machine.

The tensor values listed in Table 1 for DUMTA, DUAT, and DUAP show good correlation with one another. The six-membered ring nitroxides DUMTA and DUAT have identical values for the **g** tensor. The A_{xx} values are also the same; however, A_{yy} and A_{zz} differ slightly. This may be a consequence of the different tether lengths producing a

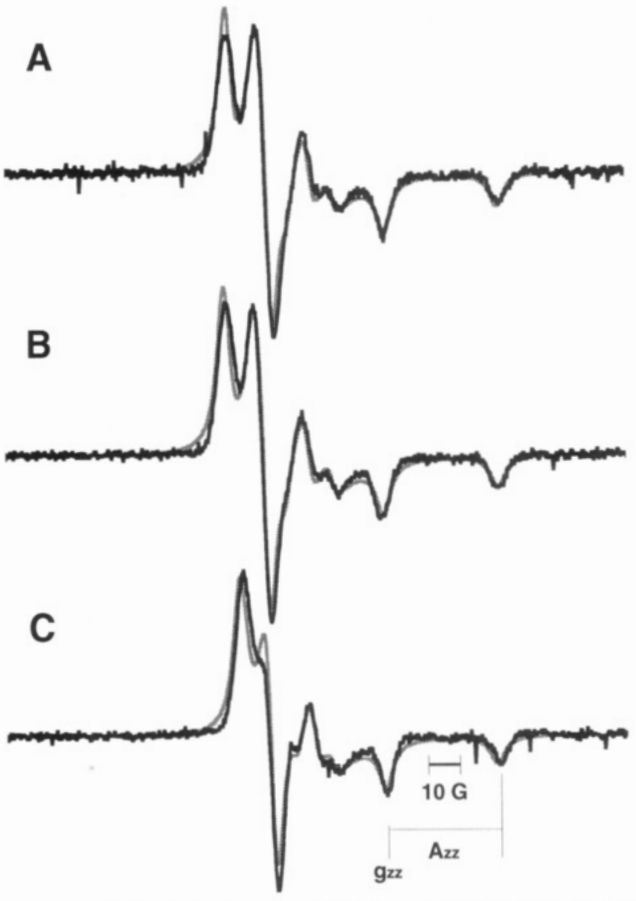

FIGURE 6: Q-band EPR spectra (200 G scan) of (A) DUMTA, (B) DUAT, and (C) DUAP. Experimental spectra are indicated by a solid black line while simulations are denoted by a gray line.

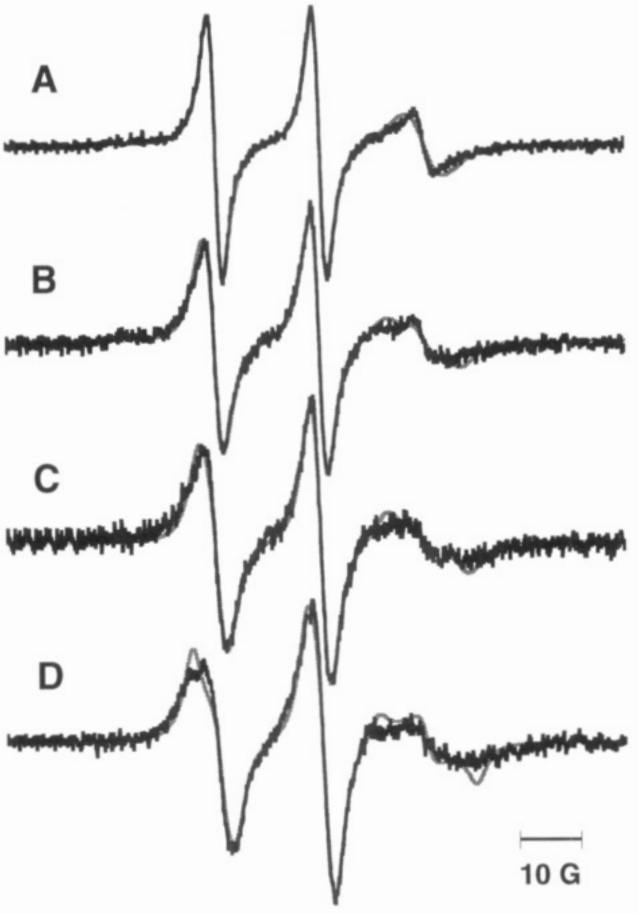

FIGURE 7: (A) $(dT)_7$DUMTA$(dT)_7$•$(dA)_{15}$, (B) $[(dT)_7$DUMTA-$(dT)_7]_2$•$(dA)_{30}$, (C) $[(dT)_7$DUMTA$(dT)_7]_3$•$(dA)_{45}$, and (D) $[(dT)_7$-DUMTA$(dT)_7]_m$•$(dA)_n$ simulated according to the dynamic cylinder model.

slightly different spin density on the ring nitrogen, or it may be the result of incomplete motional restriction. The **g** tensor traces are equivalent for these two spin labels, and the isotropic $\bar{g}$ and $\bar{A}$ values are nearly identical as well. An important test for the internal consistency of these values relies on the principle that the trace of a second-order tensor remains constant upon rotation. Variation in the trace can result from changes in solvent polarity. The criterion of rotational invariance is satisfied for these spin labels since the isotropic values obtained under conditions of rapid reorientation correlate well with the tensor traces (i.e., $^1/_3$Tr **g** and $^1/_3$Tr **A**) of the rigid-limit spectra.

The **g** tensor elements and the $\bar{g}$ value for DUAP are similar to those for DUMTA and DUAT. As expected, the values for A_{xx}, A_{yy}, A_{zz}, and $\bar{A}$ are slightly smaller for the five-membered ring compared to the six-membered ring. Comparison of the isotropic $\bar{g}$ and $\bar{A}$ values with the respective tensor traces indicates very good agreement as well.

$\bar{g}$ and $\bar{A}$ were verified for DUMTA by performing an isotropic simulation with the EPRFIT program. The correlation times, magnetic tensors, and B were allowed to vary; however, the parameters were constrained such that $g_{xx} = g_{yy} = g_{zz}$, $A_{xx} = A_{yy} = A_{zz}$, and $\tau_{\|} = \tau_{\perp}$. The tilt angle was set to zero.

The line positions of the simulation matched the experimental spectrum, but the peak shapes were different near the base line. This could be the result of either incomplete tensor averaging or the nonsphericity of the monomers. Whatever the reason for the slightly different line shapes, the simulation confirmed the values for $\bar{g}$ and $\bar{A}$.

DUMTA Simulations. The EPR spectra of the DUMTA-labeled 15mer, 30mer, 45mer, and polymer were simulated according to the dynamic cylinder model (Figure 7) and the base disk model (Figure 8). The dynamic cylinder simulations fit the data well, including the upfield manifold which is often difficult to simulate. The simulation parameters are listed in Table 2. Although 8 parameters (7 for the polymer) were allowed to vary during the simulations, there is good agreement between the four systems. It is important to note that although these simulation parameters are allowed to vary independently, they are consistent with the mathematical constraints required by the system, ensuring that they provide a unique fit.

The base disk simulations also display good conformity with the experimental spectra. The simulation of the upfield manifold is representative of the smooth average generally seen when the magnetic tensors are axially symmetric. The base disk simulation parameters are shown in Table 3.

Correlation between the Two Models. Since $\tau_{\|}$ (base disk model), θ_{dc}, and S (dynamic cylinder model) will all be constant for a given spin label, a reasonable place to start a comparison of these two models is with the helix length-dependent dynamics. It is expected that:

$$\tau_{\perp}(\text{base disk model}) \propto \tau_{rb}(\text{dynamic cylinder model}) \quad (16)$$

where τ_{rb} is defined for the DNA helix according to eq 13.

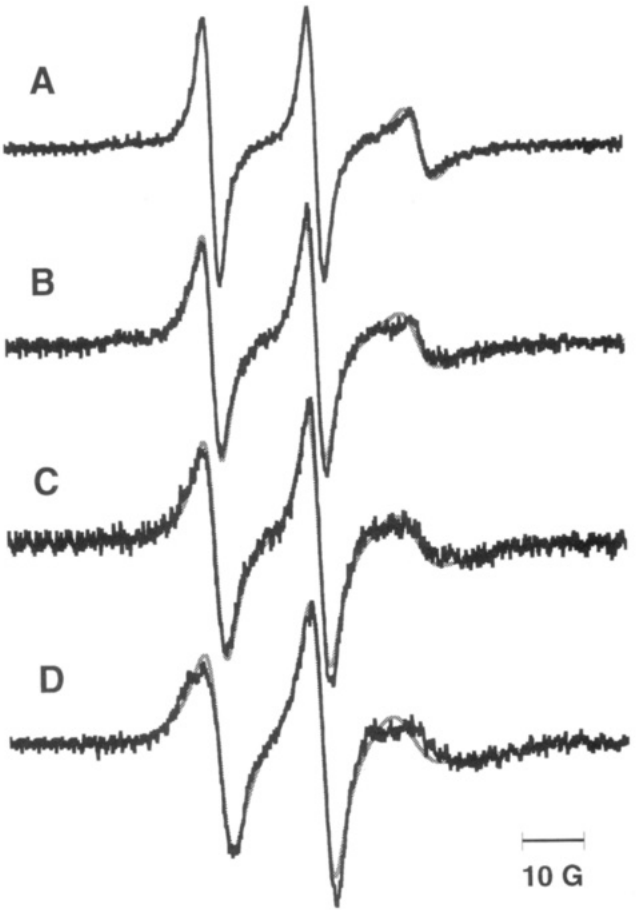

FIGURE 8: (A) $(dT)_7$DUMTA$(dT)_7$•$(dA)_{15}$, (B) [$(dT)_7$DUMTA-$(dT)_7]_2$•$(dA)_{30}$, (C) [$(dT)_7$DUMTA$(dT)_7]_3$•$(dA)_{45}$, and (D) [$(dT)_7$-DUMTA$(dT)_7]_m$•$(dA)_n$ simulated according to the base disk model.

Since τ_{rb} varies directly with the number of base pairs, the helix length dependence of τ_{rb} was compared to the helix length dependence of $\tau_\perp$ which is sensitive to both local base dynamics and global tumbling. Figure 9A demonstrates the proportional variation between $\tau_\perp$ and τ_{rb}. $\tau_\perp$ exhibits weaker helix length dependence since global tumbling is only part of the motion that it detects. The next logical step was a comparative helix length-dependent plot between $\tau_\perp$ and τ_{rb} weighted by the order parameter (Figure 9B). When $S^2\tau_{rb}$ is plotted, the variation is similar to that of $\tau_\perp$ such that:

$$\tau_\perp \propto S^2\tau_{rb} \tag{17}$$

Thus, S^2 is the appropriate weighting factor representing the degree of coupling between $\tau_\perp$ and τ_{rb}, and $S^2\tau_{rb}$ represents the fraction of global motion detected by the spin-labeled base.

DISCUSSION

Rigid-Limit Tensors. Hustedt et al. (1993a) have discussed the difficulties confronted in determining rigid-limit tensors. One particular concern is that hydrogen bonding of the nitroxide will increase the hyperfine splitting (Hwang et al., 1975). An increase in solvent polarity or a decrease in temperature will result in the formation of hydrogen-bonded complexes. A two-component approach has been described for determining the hydrogen-bonded and non-hydrogen-bonded A_{zz} values (Johnson, 1981). It is critical that the mononucleotides be strongly restricted so that motional effects will not cause any tensor averaging. At 233 K, the line positions changed very little with a further decrease in temperature, indicating that the rigid limit had been reached. However, attempts to apply the two-component model to the nitroxides described here were unsuccessful. Considering that at room temperature hydrogen bonding will occur to some extent and that the glycerol/water solvent used in these experiments has only a slightly different polarity than pure water, the effect of hydrogen-bonding on the **A** tensor was considered to be negligible. The good agreement between the isotropic $\bar{A}$ value measured in a water buffer at room temperature and $^1/_3$Tr **A** obtained in glycerol/water at −40 °C supports this conclusion. Furthermore, there is excellent accordance between the isotropic $\bar{g}$ value and $^1/_3$Tr **g** for the two environments.

The principal magnetic tensor elements obtained from the X- and Q-band measurements are self-consistent (i.e., rotationally invariant) for each spin label and display good agreement with one another despite the difficulties inherent in establishing rigid-limit tensors. The effort expended in determining these values has provided the foundation for more fully elucidating nucleic acid dynamics by EPR.

DNA Dynamics. Most of the spin-labeled nucleic acids that have been synthesized in the Bobst laboratory in the past have been polymers. The dynamics of these systems were analyzed according to the base disk model (Kao et al., 1983; Kao & Bobst, 1985; Pauly et al., 1987; Strobel et al., 1990b). Spin labels were incorporated into the nucleic acids either by random alkylation or enzymatically. However, alkylation is not site specific, and the enzyme would not accept the one-atom-tethered mononucleotides as substrates and only poorly incorporated two-atom-tethered labels (Toppin, 1983). With the advent of chemical DNA synthesis technology, one- and two-atom-tethered spin labels could be introduced into oligomers sequence specifically. Although the spectra from these oligomers indicated fast reorientation for the spin-labeled base, there was also unexpected slow motional features. Previously, comparison of the EPR spectra of a DUAT-labeled 26mer with the corresponding polymer seemed to indicate that a five-atom-tethered nitroxide did not detect any helix length dependence (Bobst et al., 1988). However, the spectra from the DUMTA-labeled 15mer, 30mer, 45mer, and polymer displayed dependence upon the helix length. Therefore, a new method of analysis was developed to account for these helix length-dependent motions. The current approach includes both global tumbling and internal dynamics in a single analysis while minimizing the required assumptions regarding the geometry of the motions.

The EPR spectra for most of the spin-labeled molecules were fit very well by the EPRFIT program. For spectra where the upfield manifold consists of more than one turning point (e.g., the DUMTA polymer) (Figure 8), the base disk model does not yield spectral simulations displaying multiple turning points. The reason for this is probably that the dynamics deviate from an axially symmetric model.

A number of criteria were met to ensure good correlation between the two approaches and uniqueness of the simulations:

Magnetic Tensors. For the dynamic cylinder model, the averaged set of **g** and **A** tensors are nearly constant as the correlation times are changed according to the Tirado and de la Torre equations. In addition, Tr **A**′ and Tr **g**′

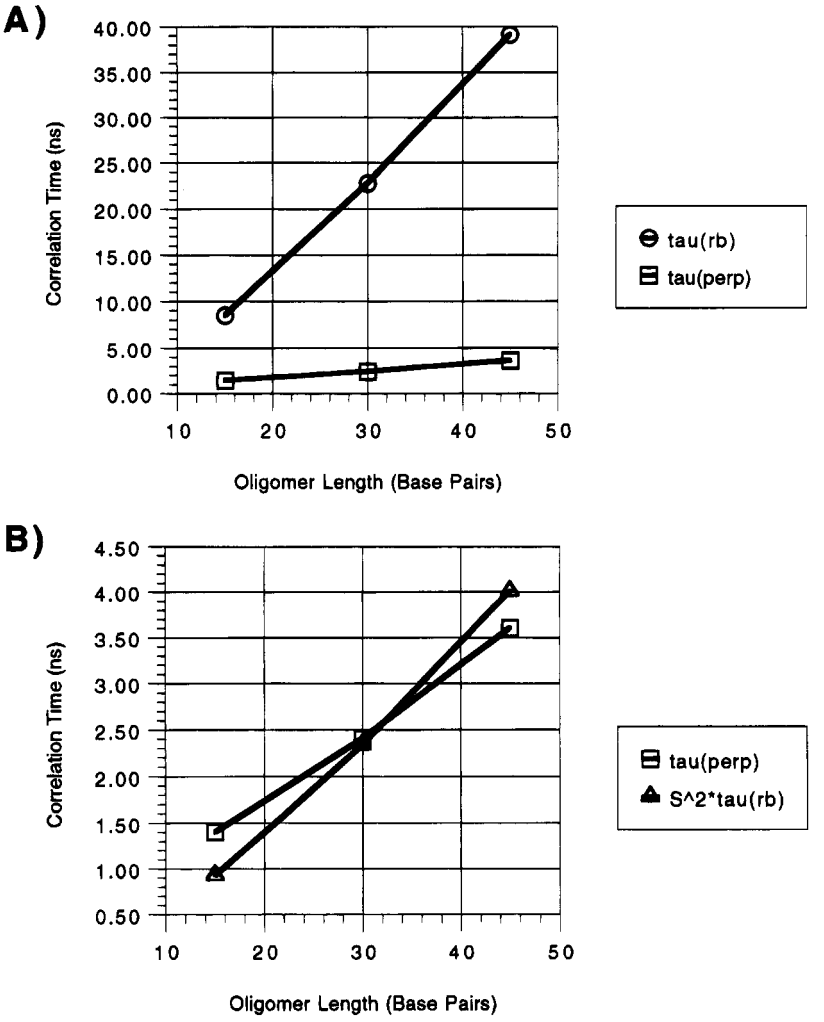

FIGURE 9: Helix length dependence of DUMTA base dynamics ($\tau_\perp$) compared to (A) global tumbling (τ_{rb}) and (B) the component of global tumbling coupled to base dynamics through the order parameter ($S^2\tau_{rb}$).

Table 2: Dynamic Cylinder Simulation Parameters

compd	g'_{xx}	g'_{yy}	g'_{zz}	A'_{xx} (G)	A'_{yy} (G)	A'_{zz} (G)	$T_{\|}$ (ns)	$T_\perp$ (ns)	θ_{dc} (deg)	B (G)
$(dT)_7DUMTA(dT)_7{\cdot}(dA)_{15}$	2.0080	2.0060	2.0049	11.5	15.8	23.1	4.7	11.4	49	1.28
$[(dT)_7DUMTA(dT)_7]_2{\cdot}(dA)_{30}$	2.0079	2.0061	2.0049	11.4	16.1	22.9	8.5	46.7	51	1.34
$[(dT)_7DUMTA(dT)_7]_3{\cdot}(dA)_{45}$	2.0077	2.0063	2.0049	11.8	16.1	23.1	12.3	118	53	1.53
$[(dT)_7DUMTA(dT)_7]_m{\cdot}(dA)_n$	2.0077	2.0061	2.0051	11.6	16.7	23.1	RL	RL	n/a	1.88

Table 3: Base Disk Simulation Parameters

compd	g_{xx}	g_{yy}	g_{zz}	A_{xx} (G)	A_{yy} (G)	A_{zz} (G)	$\tau_{\|}$ (ns)	$\tau_\perp$ (ns)	θ_{bd} (deg)	B (G)
$(dT)_7DUMTA(dT)_7{\cdot}(dA)_{15}$	2.0096	2.0067	2.0028	7.47	7.21	36.3	0.50	1.4	40	0.8
$[(dT)_7DUMTA(dT)_7]_2{\cdot}(dA)_{30}$	2.0096	2.0067	2.0028	7.47	7.21	36.3	0.50	2.4	40	0.8
$[(dT)_7DUMTA(dT)_7]_3{\cdot}(dA)_{45}$	2.0096	2.0067	2.0028	7.47	7.21	36.3	0.50	3.6	40	0.8
$[(dT)_7DUMTA(dT)_7]_m{\cdot}(dA)_n$	2.0096	2.0067	2.0028	7.47	7.21	36.3	0.50	6.2	40	0.8

correspond to Tr **A** and Tr **g**, respectively, in agreement with the fact that the trace of a second-order tensor is rotationally invariant (Table 4).

Correlation Times. For the base disk model, $\tau_{\|}$ is a constant representative of the particular tether length of the spin label. The values of $\tau_{\|}$ are in very good agreement with what is expected for the individual spin labels based upon results obtained with other tether lengths.

Tilt Angle. The tilt angle θ is defined as the angle between the principal diffusion axis z' and the principal magnetic axis z. Since the principal diffusion axes for the two simulation approaches are approximately perpendicular to one another, the sum of the tilt angles for the two approaches should be about 90°. This was accomplished since $\theta_{bd} = 40°$ for the base disk simulations and $\theta_{dc} \cong 50°$ for the dynamic cylinder simulations. For the base disk simulations, $\tau_\perp$ becomes increasingly sensitive to the value of the tilt angle as the difference between $\tau_{\|}$ and $\tau_\perp$ increases (e.g., when the DNA helix becomes longer).

The values for θ_{bd} and θ_{dc} were chosen for the following reasons: (1) Over 40 spin-labeled systems have been analyzed according to the base disk model (Kao et al., 1983; Kao & Bobst, 1985; Pauly et al., 1987; Strobel et al., 1990b), yielding values of θ_{bd} between 40° and 55°. (2) θ_{dc} was

Table 4: Rotational Invariance of Magnetic Tensors

compd	$\bar{g}$	$^1/_3$Tr **g**	$^1/_3$Tr **g**′	$\bar{A}$ (G)	$^1/_3$Tr **A** (G)	$^1/_3$Tr **A**′ (G)
$(dT)_7$DUMTA$(dT)_7$•$(dA)_{15}$	2.0063	2.0064	2.0063	16.9	17.0	16.8
$[(dT)_7$DUMTA$(dT)_7]_2$•$(dA)_{30}$	2.0063	2.0064	2.0063	16.9	17.0	16.8
$[(dT)_7$DUMTA$(dT)_7]_3$•$(dA)_{45}$	2.0063	2.0064	2.0063	16.9	17.0	17.0
$[(dT)_7$DUMTA$(dT)_7]_m$•$(dA)_n$	2.0063	2.0064	2.0063	16.9	17.0	17.1

Table 5: Dynamic Cylinder Model Results

compd	τ_{rb} (ns)	S_g	S	S_z	$S^2\tau_{rb}$ (ns)
$(dT)_7$DUMTA$(dT)_7$•$(dA)_{15}$	8.5	0.39	0.33	0.33	0.93
$[(dT)_7$DUMTA$(dT)_7]_2$•$(dA)_{30}$	22.8	0.39	0.32	0.32	2.33
$[(dT)_7$DUMTA$(dT)_7]_3$•$(dA)_{45}$	39.1	0.39	0.32	0.32	4.00
$[(dT)_7$DUMTA$(dT)_7]_m$•$(dA)_n$		0.34	0.31	0.31	

allowed to float for the dynamic cylinder model DUMTA simulations from which a value of 51 ± 2° was obtained.

The most difficult problem in interpreting the EPR spectra is the extraction of the experimental correlation times. Because the line shapes do not consist of three Lorentzian lines, the correlation times must be determined by simulating the entire line shape. Combining the base disk model with the dynamic cylinder model not only allows global and internal dynamics to be monitored and analyzed separately but also confirms the approximate values of $\tau_{||}$ and $\tau_\perp$. The proportionality developed in eq 17 and verified in Figure 9B strongly supports this approach.

The order parameter can be calculated in several ways. The form of eq 8 was preferred since it takes into account all three principal values of the hyperfine tensor. However, the order parameter is often reported with respect to the z-components (eq 9). Results from both of these equations are listed in Table 5, indicating that they are equal for these systems. S_g was calculated by substituting the **g** tensors into eq 9. Since the **g** and **A** tensors should both average to the same degree, comparison of S_g with S provides another consistency test. The values shown in Table 5 demonstrate that both tensors provide similar order parameters. The small differences are due to the fact that **g** tensor values are difficult to measure accurately, which explains why the order parameter is generally calculated using the **A** tensor.

An important requirement of the spin-labeling technique is that the probe accurately report dynamics. In the present case, the results indicate that the nitroxide is coupled to base motion and is not simply wobbling in the major groove. Currently, over 40 spin-labeled systems have been consistently analyzed with the base disk model (Kao et al., 1983; Kao & Bobst, 1985; Pauly et al., 1987; Strobel et al., 1990b). In all of these systems, $\tau_\perp$ has been found to be essentially independent of tether length while $\tau_{||}$ has shown tether dependence. Single strand to double strand interconversion is clearly monitored by spin labels, which fits quite well with the interpretation that base dynamics are being detected. The ability to monitor the B−Z conformational transition further confirms that the nitroxide monitors base motion (Strobel et al., 1990a,b). Specifically, as the DNA helix undergoes a transition from the right- to the left-handed form, the bases swing toward the surface of the helix, which places the nitroxide further from the helix. Molecular models showing this phenomenon have been published previously (Figure 3, Strobel et al., 1990a). Thus, in the absence of coupling, $\tau_\perp$ would be expected to decrease as a result of less hindered motion of the probe. The experimental line shape obtained with 5-atom- and 11-atom-tethered nitroxides clearly indicates the presence of a more hindered motion.

Application of the dynamic cylinder model to the earlier B−Z experimental data (Strobel et al., 1990b) illustrates that S changes in response to conformational transitions. Dynamic cylinder simulations of the B and Z forms of $(dG\text{-}dC)_n$ labeled with a five-atom-tethered nitroxide yield order parameters of 0.15 and 0.26, respectively (Keyes & Bobst, 1995). This local ordering is consistent with the finding that Z-DNA is more rigid than B-DNA (Thomas & Bloomfield, 1983).

CONCLUSION

The approach to interpreting nucleic acid dynamics developed in this paper provides a correlation between two motional models, each of which yields insight into the internal dynamics. The order parameter provides a quantitative measure of base motions without requiring the geometry of that motion. The base disk model is applied in conjunction with the dynamic cylinder model, indicating that the value of $\tau_\perp$ determined in this work correlates well with both τ_{rb} and the order parameter such that $\tau_\perp \propto S^2\tau_{rb}$. The parameters S (internal dynamics) and $\tau_\perp$ (internal and global dynamics) are useful measures of motional changes and provide a means to studying spin-labeled nucleic acid conformational changes (e.g., B−Z transition) and size-dependent phenomena (e.g., protein binding).

ACKNOWLEDGMENT

We would like to thank Elizabeth Bobst for assistance with the experimental work, Chris Felix at the National Biomedical ESR Center for guidance with the Q-band measurements, and Frank Meeks and Attila Szabo for beneficial discussions concerning theoretical aspects of this work. We also thank Eric Hustedt for providing us with the EPRFIT program and for helpful discussions regarding its programming and operation.

REFERENCES

Allison, S. A., & Schurr, J. M. (1979) *Chem. Phys. 41*, 35.
Bales, B. L. (1989) in *Spin Labeling: Theory and Applications, Vol. 8 of Biological Magnetic Resonance* (Berliner, L. J., & Reuben, J., Eds.) p 77, Plenum, New York.
Barkley, M. D., & Zimm, B. H. (1979) *J. Chem. Phys. 70*, 2991.
Berliner, L. J., Ed. (1976) *Spin Labeling: Theory and Applications*, p 564, Academic Press, New York.
Bobst, A. M. (1979) in *Spin Labeling II: Theory and Applications* (Berliner, L. J., Ed.) p 291, Academic Press, New York.
Bobst, A. M., Ireland, J. C., & Bobst, E. V. (1984) *J. Biol. Chem. 259*, 2130.
Bobst, A. M., Pauly, G. T., Keyes, R. S., & Bobst, E. V. (1988) *FEBS Lett. 228*, 33.
Borer, P. N., LaPlante, S. R., Kumar, A., Zanatta, N., Martin, A., Hakkinen, A., & Levy, G. C. (1994) *Biochemistry 33*, 2441.
Broersma, S. (1960) *J. Chem. Phys. 32*, 1626.
Eimer, W., Williamson, J. R., Boxer, S. G., & Pecora, R. (1990) *Biochemistry 29*, 799.

Englander, S. W., & Kallenbach, N. R. (1984) *Q. Rev. Biophys. 16*, 521.
Folta-Stogniew, E., & Russu, I. M. (1994) *Biochemistry 33*, 11016.
Freed, J. H. (1976) in *Spin Labeling: Theory and Applications* (Berliner, L. J., Ed.) p 53, Academic Press, New York.
Freed, J. H. (1977) *J. Chem. Phys. 66*, 4183.
Froehler, B. C., Wadwani, S., Terhorst, T. J., & Gerrard, S. R. (1992) *Tetrahedron Lett. 33*, 5307.
García de la Torre, J., & Bloomfield, V. A. (1981) *Q. Rev. Biophys. 14*, 81.
Goljer, I., & Bolton, P. H. (1994) in *Two-Dimensional NMR Spectroscopy* (Croasmun, W. R., & Carlson, R. M. K., Eds.) 2nd ed., p 699, VCH Publishers, New York.
Griffith, O. H., & Jost, P. C. (1976) in *Spin Labeling: Theory and Applications* (Berliner, L. J., Ed.) p 453, Academic Press, New York.
Griffith, O. H., Cornell, D. W., & McConnell, H. M. (1965) *J. Chem. Phys. 43*, 2909.
Hartmann, B., Leng, M., & Ramstein, J. (1986) *Biochemistry 25*, 3073.
Hustedt, E. J., Spaltenstein, A., Kirchner, J. J., Hopkins, P. B., & Robinson, B. H. (1993a) *Biochemistry 32*, 1774.
Hustedt, E. J., Cobb, C. E., Beth, A. H., & Beechem, J. M. (1993b) *Biophys. J. 64*, 614.
Hwang, J. S., Mason, R. P., Hwang, L.-P., & Freed, J. H. (1975) *J. Phys. Chem. 79*, 489.
Hyde, J. S., Newton, M. E., Strangeway, R. A., Camenisch, T. G., & Froncisz, W. (1991) *Rev. Sci. Instrum. 62*, 2969.
Johnson, M. E. (1981) *Biochemistry 20*, 3319.
Kao, S.-C., & Bobst, A. M. (1985) *Biochemistry 24*, 5465.
Kao, S.-C., Polnaszek, C. F., Toppin, C. R., & Bobst, A. M. (1983) *Biochemistry 22*, 5563.
Keyes, R. S., & Bobst, A. M. (1993) *Biophys. Chem. 45*, 281.
Keyes, R. S., & Bobst, A. M. (1995) *Biophys. J. 68*, A103.
Kryak, D. D. (1990) Sequence Specific Incorporation of Deoxyuridylic Acid Substituted in Position 5 with Two-Atom-Tethered Nitroxides into Oligothymidylic Acids by Phosphotriester Chemistry, Ph.D. Dissertation, University of Cincinnati.
Kryak, D. D., & Bobst, A. M. (1990) *Nucleosides Nucleotides 9*, 1015.
Lipari, G., & Szabo, A. (1982) *J. Am. Chem. Soc. 104*, 4546.
Mason, R. P., Polnaszek, C. F., & Freed, J. H. (1974) *J. Phys. Chem. 78*, 1324.
Nordio, P. L. (1976) in *Spin Labeling: Theory and Applications* (Berliner, L. J., Ed.) p 5, Academic Press, New York.
Pan, Y.-C. E. (1975) A Spin Label Approach for Studying Nucleic Acid–Nucleic Acid and Nucleic Acid–Protein Interactions, Ph.D. Dissertation, University of Cincinnati.
Pasenkiewicz-Gierula, M., Hyde, J. S., & Pilbrow, J. R. (1983) *J. Magn. Reson. 55*, 255.
Patkowski, A., Eimer, W., & Dorfmüller, Th. (1990) *Biopolymers 30*, 975.
Pauly, G. T., Thomas, I. E., & Bobst, A. M. (1987) *Biochemistry 26*, 7304.
Pauly, G. T., Bobst, E. V., Bruckman, D., & Bobst, A. M. (1989) *Helv. Chim. Acta 72*, 110.
Polnaszek, C. F. (1976) An Electron Spin Resonance Study of Rotational Reorientation and Spin Relaxation in Liquid Crystal Media, Ph.D. Dissertation, Cornell University.
Polnaszek, C. F., & Freed, J. H. (1975) *J. Phys. Chem. 79*, 2283.
Robinson, B. H., Lerman, L. S., Beth, A. H., Frisch, H. L., Dalton, L. R., & Auer, C. (1980) *J. Mol. Biol. 139*, 19.
Schneider, D. J., & Freed, J. H. (1989a) in *Spin Labeling: Theory and Applications, Volume 8 of Biological Magnetic Resonance* (Berliner, L. J., & Reuben, J., Eds.) p 1, Plenum, New York.
Schneider, D. J., & Freed, J. H. (1989b) in *Lasers, Molecules, and Methods, Volume 73 of Advances in Chemical Physics* (Hirschfelder, J. O., Wyatt, R. E., & Coalson, R. D., Eds.) p 387, Wiley, New York.
Schurr, J. M., & Schmitz, K. S. (1986) *Annu. Rev. Phys. Chem. 37*, 271.
Spaltenstein, A., Robinson, B. H., & Hopkins, P. B. (1988) *J. Am. Chem. Soc. 110*, 1299.
Spaltenstein, A., Robinson, B. H., & Hopkins, P. B. (1989) *Biochemistry 28*, 9484.
Steinhoff, H.-J. (1988) *J. Biochem. Biophys. Methods 17*, 237.
Steinhoff, H.-J., Lieutenant, K., & Schlitter, J. (1989) *Z. Naturforsch. 44c*, 280.
Strobel, O. K., Keyes, R. S., & Bobst, A. M. (1990a) *Biochem. Biophys. Res. Commun. 166*, 1435.
Strobel, O. K., Keyes, R. S., & Bobst, A. M. (1990b) *Biochemistry 29*, 8522.
Strobel, O. K., Kryak, D. D., Bobst, E. V., & Bobst, A. M. (1991) *Bioconjugate Chem. 2*, 89.
Thomas, T. J., & Bloomfield, V. A. (1983) *Nucleic Acids Res. 11*, 1919.
Tidor, B., Irikura, K. K., Brooks, B. R., & Karplus, M. (1983) *J. Biomol. Struct. Dyn. 1*, 231.
Tirado, M. M., & de la Torre, J. G. (1980) *J. Chem. Phys. 73*, 1986.
Toppin, C. R. (1983) Synthesis of Analogues of Uridine and 2′-Deoxyuridine Spin Labelled at Positions 4 or 5 as Substrates for RNA and DNA Polymerizing Enzymes, Ph.D. Dissertation, University of Cincinnati.
Toppin, C. R., Pauly, G. T., Devanesan, P. D., Kryak, D. D., & Bobst, A. M. (1986) *Helv. Chim. Acta 69*, 345.
Van, S. P., Birrell, G. B., & Griffith, O. H. (1974) *J. Magn. Reson. 15*, 444.
Wahl, Ph., Paoletti, J., & Le Pecq, J.-B. (1970) *Proc. Natl. Acad. Sci. U.S.A. 65*, 417.
Wells, R. D. (1988) *J. Biol. Chem. 263*, 1095.
Woessner, D. E. (1962) *J. Chem. Phys. 37*, 647.
Zager, S. A., & Freed, J. H. (1982) *J. Chem. Phys. 77*, 3344.
Zimmel, J. M. (1983) Motion of Rodlike Molecules, Ph.D. Dissertation, University of Minnesota.

BI950550N